Neurobiology of Disease

Downregulating PTBP1 Fails to Convert Astrocytes into Hippocampal Neurons and to Alleviate Symptoms in Alzheimer's Mouse Models

Tiantian Guo,[1*] Xinjia Pan,[1*] Guangtong Jiang,[1] Denghong Zhang,[1] Jinghui Qi,[1] Lin Shao,[1] Zhanxiang Wang,[1] Huaxi Xu,[1,2] and Yingjun Zhao[1]

[1]Center for Brain Sciences, First Affiliated Hospital of Xiamen University, Institute of Neuroscience, Fujian Provincial Key Laboratory of Neurodegenerative Disease and Aging Research, School of Medicine, Xiamen University, Xiamen, Fujian 361005, China, and [2]Institute for Brain Science and Disease, Chongqing Medical University, Chongqing 400016, China

Conversion of astroglia into functional neurons has been considered a promising therapeutic strategy for neurodegenerative diseases. Recent studies reported that downregulation of the RNA binding protein, polypyrimidine tract-binding protein 1 (PTBP1), converts astrocytes into neurons *in situ* in multiple mouse brain regions, consequently improving pathologic phenotypes associated with Parkinson's disease, RGC loss, and aging. Here, we demonstrate that PTBP1 downregulation using an astrocyte-specific AAV-mediated shRNA system fails to convert hippocampal astrocytes into neurons in both male and female wild-type (WT) and β-amyloid (5×FAD) and tau (PS19) Alzheimer's disease (AD) mouse models and fails to reverse synaptic/cognitive deficits and AD-associated pathology in male mice. Similarly, PTBP1 downregulation cannot convert astrocytes into neurons in the striatum and substantia nigra in both male and female WT mice. Together, our study suggests that cell fate conversion strategy for neurodegenerative disease therapy through manipulating one single gene, such as PTBP1, warrants more rigorous scrutiny.

Key words: **Alzheimer's disease; astrocyte; cell fate conversion; glia; transdifferentiation**

Significance Statement

Our results do not support some of the recent extraordinary and revolutionary claims that resident astrocytes can be directly and efficiently converted into neurons. Our study is critical for the field of neural regeneration and degeneration. In addition, our study is financially important because it may prevent other researchers/organizations from wasting a vast amount of time and resources on relevant investigations.

Introduction

Neuronal loss is the primary cause for functional deterioration in the CNS in neurodegenerative diseases such as Parkinson's disease (PD) and Alzheimer's disease (AD; Mesulam, 1999; Kalia and Lang, 2015). Replenishment of neurons is considered an effective approach to restore CNS function. Two major regeneration strategies using neuronal lineage cells have been developed so far, transplantation of exogenous iPSC-derived neuronal cells and activation of endogenous neurogenesis niche. However, transplantation of exogenous cells may induce immunologic rejection and tumorigenesis (Olanow et al., 2003; Trounson and McDonald, 2015). Adult neurogenesis only occurs in a few small brain regions in rodent models, and whether it exists in humans remains controversial (Mu and Gage, 2011; Kempermann et al., 2018; Gage, 2019) In pursuing novel approaches for neuronal replenishment, attempts have been made to transdifferentiate residential glia cells into functional neurons (Grande et al., 2013; Guo et al., 2014; Liu et al., 2015; Niu et al., 2015; Torper et al., 2015; Matsuda et al., 2019; Mattugini et al., 2019; Chen et al., 2020; Qian et al., 2020; Zhou et al., 2020; Lentini et al., 2021; Maimon et al., 2021; Tai et al., 2021). The *in situ* glia-to-neuron conversion represents an ideal strategy for neuronal regeneration because (1) glial cells including astrocytes and microglia are overproliferated and become reactive (a process termed as gliosis), leading to

Received June 1, 2022; revised July 21, 2022; accepted Aug. 2, 2022.

Author contributions: T.G., H.X., and Y.Z. designed research; T.G., X.P., G.J., D.Z., J.Q., L.S., and Z.W. performed research; T.G. and X.P. analyzed data; T.G., H.X., and Y.Z. wrote the paper.

This study was supported by Ministry of Science and Technology of the People's Republic of China Grants 2021YFA1101401 (Y.Z.) and 2021ZD0202402 (H.X.); the National Natural Science Foundation of China Grants 82071213 (Y.Z.), 92049202, and 92149303 (H.X.); and start-up funding from Xiamen University (Y.Z.). We thank Baoying Xie, Haiping Zheng, Yixian Gao, Xiang You, Qingfeng Liu, Lei Huang, and Jingru Huang at Xiamen University for technical assistance.

*T.G. and X.P. contributed equally to this work.

The authors declare no competing interests.

Correspondence should addressed to Huaxi Xu at Huaxi.Xu@MolecularNeurodegeneration.org or Yingjun Zhao at yjzhao@xmu.edu.cn.

https://doi.org/10.1523/JNEUROSCI.1060-22.2022

Copyright © 2022 the authors

neuroinflammation during neurodegeneration, and (2) neurons can be regenerated from the excessive glia in designated brain regions where neuronal loss occurs.

Among the targets for converting astroglia into neurons, polypyrimidine tract-binding protein 1 (PTBP1) has attracted much attention, because downregulation of this single protein has been indicated to be sufficient to directly convert astrocytes into functional neurons with high efficiencies within several weeks to months (Qian et al., 2020; Zhou et al., 2020; Maimon et al., 2021). Specifically, downregulation of PTBP1 by adeno-associated virus (AAV)-mediated shRNA system or antisense oligonucleotides (ASO) converted midbrain astrocytes to dopaminergic neurons and reversed motor deficits in a chemically induced PD mouse model (Qian et al., 2020). Similar motor function improvement was observed in the PD mice when striatal astrocytes were converted into functional neurons by CRISPR-CasRx-mediated PTBP1 downregulation (Zhou et al., 2020). In addition, injection of ASO targeting *Ptbp1* into CSF generated new functional cortical or hippocampal neurons in both young and aged mice (Maimon et al., 2021). Those results, should they be sustained, would represent a revolutionary advancement in therapeutics for neurodegenerative diseases.

In the current study, using an astrocyte-restrictive AAV shRNA system, we examine whether the reported astrocyte-to-neuron conversion induced by PTBP1 downregulation can happen in the hippocampus and consequently rescue synaptic and cognitive impairments in AD-associated mouse models, namely amyloid (5×FAD) and tau (neurofibrillary tangle; PS19) models. In addition, we re-examine whether PTBP1 knockdown can efficiently convert astrocytes into neurons in the brain regions of substantia nigra and striatum, as previously reported.

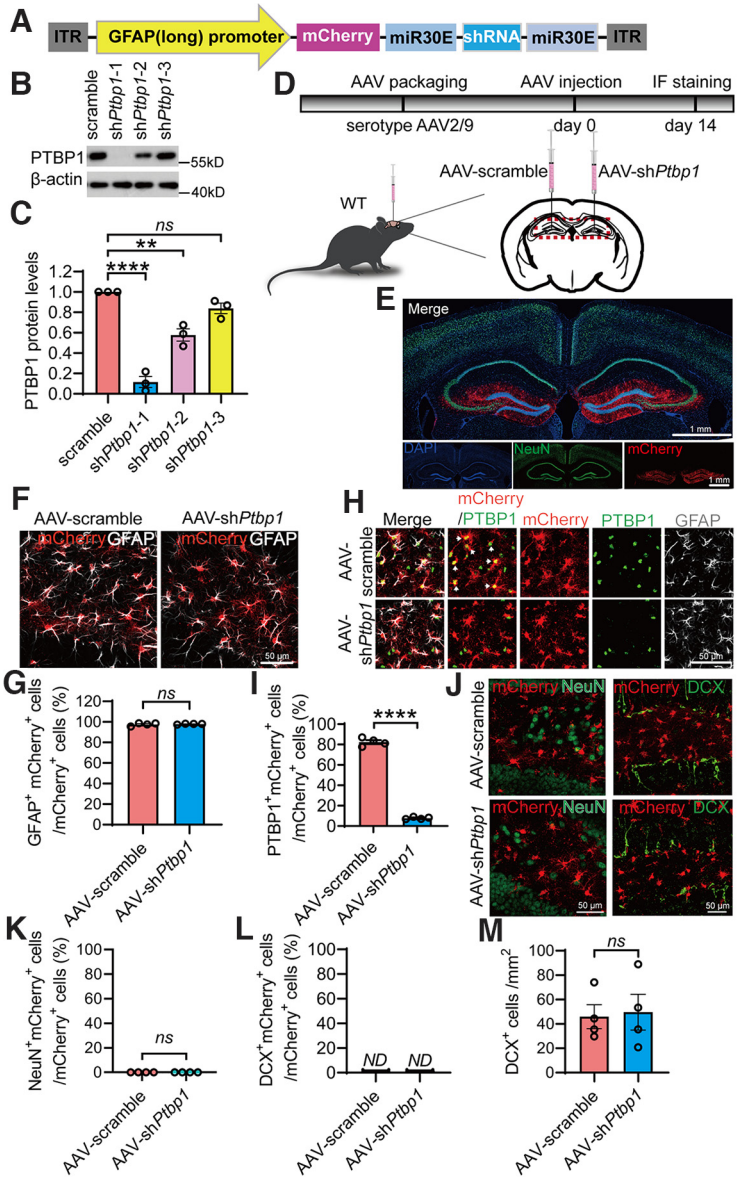

Figure 1. Specific knockdown of PTBP1 in astrocytes fails to convert hippocampal astrocytes into neurons in WT mice. ***A***, Schematic of the AAV-shRNA vector used in this study. ***B***, ***C***, Western blot analysis of PTBP1 expression in mouse primary astrocytes 7 d post-AAV transduction. Representative PTBP1 blots (***B***), quantification (***C***); $n = 3$ independent experiments, one-way ANOVA with Tukey's multiple comparisons. ***D***, Flowchart of study design to assess PTBP1 downregulation in mouse hippocampus. ***E***, Confocal images of the mouse hippocampus and cortex 2 weeks after the AAV injection. ***F***, ***G***, Confocal analysis of mCherry expression in $GFAP^+$ cells. Representative images (***F***), quantification; $n = 4$ animals, unpaired *t* test (***G***). ***H***, ***I***, Confocal analysis of PTBP1 expression in $mCherry^+$ cells. Representative images (***H***), quantification (***I***); $n = 4$ animals, unpaired *t* test. ***J–M***, Confocal analysis of fluorescent cells. Representative images (***J***), quantification (***K–M***); $n = 4$ animals, unpaired *t* test. All quantified data are represented as mean ± SEM; $^{**}p < 0.01$, $^{****}p < 0.0001$. *ns*, Not significant; *ND*, not detectable.

Materials and Methods

Experimental design

The objective of this study was to examine whether PTBP1 downregulation can convert hippocampal astrocytes into mature neurons and thereby improve symptoms of AD mouse models. An astrocyte-restrictive AAV shRNA system was used to specifically knock down astrocytic PTPB1. Immunofluorescence (IF) staining was used to assess the effect of PTPB1 downregulation on astrocyte-to-neuron conversion and AD-associated pathology. Behavioral tests and electrophysiological analysis were used to determine mouse cognitive and synaptic function. To investigate whether PTBP1 induces astrocyte-to-neuron conversion in a brain-region-specific manner, astrocytic PTBP1 in striatum and substantia nigra was downregulated by AAV-shRNA, and the situation of astrocyte-to-neuron conversion was determined.

Animals

Wild-type C57BL/6J mice were obtained from the Laboratory Animal Center at Xiamen University. The 5×FAD mice (stock #034840-JAX) and PS19 mice (stock #008169) were obtained from The Jackson Laboratory and were backcrossed into the C57BL/6J for 10 generations (https://mice.jax.org/). Only male mice were used in behavioral tests,

and both male and female mice were used in immunohistochemistry. Mice were randomly grouped by genotype and age. Experiments were conducted and analyzed in a double-blind manner. All animal studies were performed according to the protocols approved by the Institutional Animal Care and Use Committee of Xiamen University.

Isolation and culture of primary mouse astrocytes

A modified protocol was used (Schildge et al., 2013). Cortical and hippocampal tissues were dissected from postnatal day 1–2 pups and dissociated with 0.05% trypsin for 30 min at 37°C. Tissues were centrifuged for 5 min at 500 × *g* and mechanically dissociated in DMEM/F12 growth media conaining 20% FBS and 1% penicillin/streptomycin. Cells were passed through a 70 μm cell strainer, centrifuged at 500 × *g* for 3 min, and resuspended in the growth media. Cells were plated into 175 cm^2 flasks coated with 0.1% poly-L-lysine (catalog #P6282, Sigma-Aldrich) for proliferation. To examine the efficiency of AAV-mediated PTBP1 downregulation *in vitro*, cells were replated into six-well plates, transduced with the AAV and lyzed 7 d after the transduction.

Western blot analysis

Western blot was performed as previously described (Wang et al., 2006; Zeng et al., 2019). Briefly, primary cultured astrocytes were lysed in RIPA buffer (150 mM NaCl, 50 mM Tris-HCl, pH 8.0, 2 mM EDTA, 1% NP-40, 0.1% SDS, 0.5% sodium deoxycholate) containing protease inhibitor cocktail (catalog #04693132001, Roche). Equal amounts of total proteins (20 μg per sample) from the lysates were resolved by SDS-PAGE. The samples were then probed with the primary antibodies against PTBP1(rabbit, 1:1000; catalog #PA581297, Thermo Fisher Scientific) and β-actin (mouse, 1:5000; catalog #TA-09, OriGene), followed by HRP-conjugated secondary antibodies against rabbit or mouse IgG (1:5000; catalog #7074S or #7076S, Thermo Fisher Scientific).

Vectors and AAV production

To generate astrocyte-specific AAV expression vectors, shRNAs targeting mouse *Ptbp1* or scrambled shRNA was inserted into an AAV vector driven by the 2.2 kb long human *GFAP* promoter (*pAAV-GFAP-mCherry-miR30E*; VectorBuilder, https://www.vectorbuilder.cn/design/retrieve.html, VB200627-1109ntb). The sequences of shRNA-2 and shRNA-3 were obtained from VectorBuilder (https://www.vectorbuilder.cn/design/pRP_shRNA.html), whereas shRNA-1 sequence was designed based on a recent study (Qian et al., 2020). The target sequences of shRNAs and scramble were as follows: scramble, 5′-ACCTA AGGTT AAGTC GCCCT CG-3′; sh*Ptbp1*-1, 5′-GGGTG AAGAT CCTGT TCAAT A-3′; shP*tbp1*-2, 5′-TGACC TTACA GACCA GAGAT TT-3′; sh*Ptbp1*-3, 5′-ACACT ATGGT TAACT ACTAT AC-3′.

AAV viruses were produced following a well-established protocol with minor modifications (Challis et al., 2019). Briefly, HEK293T cells (catalog #CRL-3216, ATCC) were transfected with the pAAV-shRNA, pAAV2/9 Helper (catalog #112865, Addgene), and pAd-deltaF6 (catalog #112867, Addgene) plasmids. Three days post-transfection, viral particles were collected from the media and lysates of the cells and purified by iodixanol gradient ultracentrifugation in a Beckman L-100XP centrifuge with type 70 Ti rotor at 350,000 × *g* for 2 h 25 min at 18°C.

Stereotactic injection

Stereotactic injection was performed as described previously (Wang et al., 2013; Zhao et al., 2015). Briefly, after anesthetization with Avertin, the experimental mice were shaved to remove the head hairs and secured in an automated stereotaxic injection apparatus (RWD Life Science). AAV-sh*Ptbp1* or AAV-scramble (2 μl, titer 1×10^{12} viral genomes/ml) viruses were injected into the following coordinates: for hippocampal dentate gyrus, −2.5 mm anteroposterior (AP) from the bregma, ±2.0 mm mediolateral (ML), −2.4 mm dorsoventral (DL); for striatum, −0.8 mm AP from the bregma, ±1.6 mm ML, −2.8 mm DV; for substantia nigra, −3.0 mm AP from the bregma, ±1.2 mm ML, −4.6 mm DL.

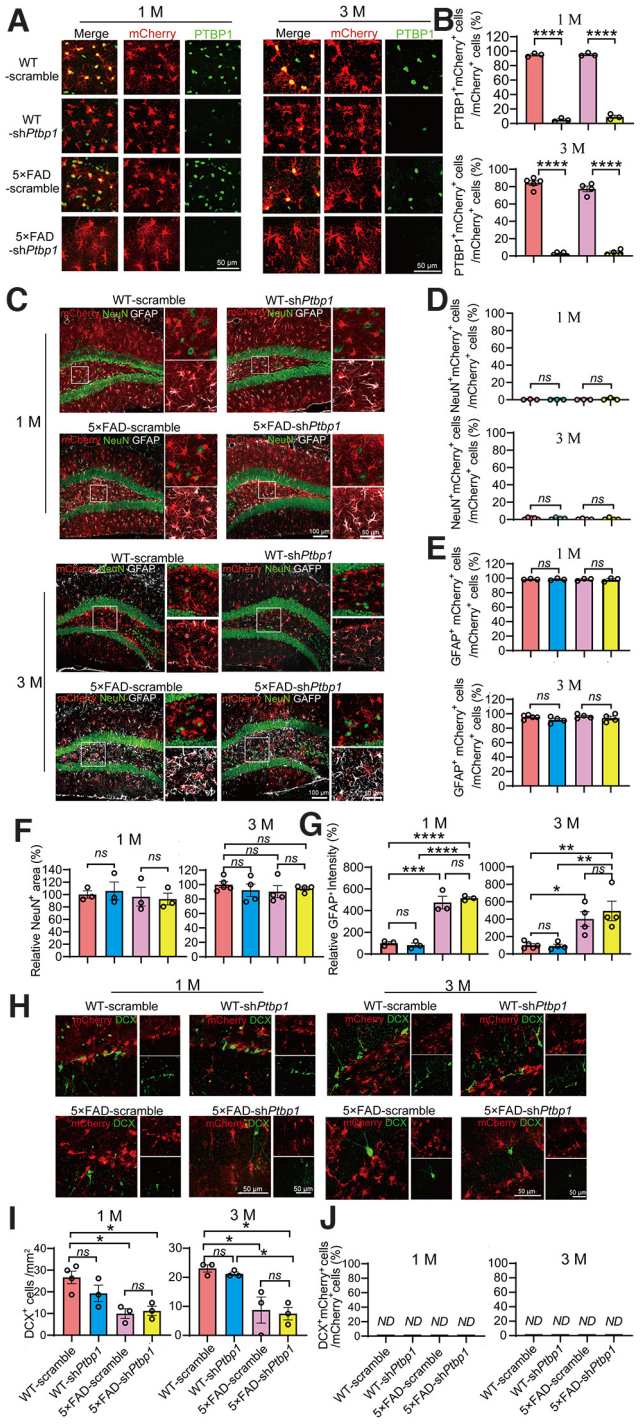

Figure 2. Downregulation of PTBP1 is not able to convert astrocytes into neurons in the hippocampus of 5×FAD mice 1 and 3 months (M) after the AAV transduction. ***A***, ***B***, Confocal analysis of PTBP1 expression in mCherry$^+$ cells in the hippocampus of 5×FAD and WT control mice 1 and 3 months after sh*Ptbp1* or the scramble control AAV transduction. Representative images (***A***), quantification (***B***); 1 M, $n = 3$ animals per group, unpaired *t* test; 3 M, $n = 4$–5 animals, unpaired *t* test. ***C***, ***G***, Confocal analysis of fluorescent cells. Representative images (***C***), quantification (***D–G***); 1 M, $n = 3$ animals, one-way ANOVA with Tukey's multiple comparisons; 3 M, $n = 4$–5 animals, one-way ANOVA with Tukey's multiple comparisons. ***H–J***, Confocal analysis of mCherry$^+$ cells and DCX$^+$ cells. Representative images (***H***), quantification (***I,J***); 1 M, $n = 3$–4 animals, one-way ANOVA with Tukey's multiple comparisons; 3 M, $n = 3$ animals per group, one-way ANOVA with Tukey's multiple comparisons. All quantified data are represented as mean ± SEM; *$p < 0.05$, **$p < 0.01$, ***$p < 0.001$, ****$p < 0.0001$. *ns*, Not significant; *ND*, not detectable.

Immunofluorescence staining

Mice were anesthetized with Avertin followed by intracardial perfusion with PBS and 4% paraformaldehyde (PFA) in PBS. Mouse brains were dissected quickly, postfixed with 4% PFA overnight at 4°C, and dehydrated with 30% sucrose in PBS until it completely settled. The brains were then encased in optimal cutting temperature compound (catalog #4583, Sakura) and cut into serial frozen sections (30–40 μm) using a cryostat (model CM1950, Leica). The sections were permeabilized and blocked with PBS containing 0.3% Triton X-100 and 10% normal donkey serum for 45 min at room temperature. The sections were incubated with the following primary antibodies at 4°C overnight: mouse anti-GFAP (1:500; catalog #3670S, Cell Signalling Technology), rabbit anti-NeuN (1:500; catalog #24307, Cell Signalling Technology), mouse anti-NeuN (1:1000; catalog #ab104224, Abcam), rabbit anti-PTBP1 (1:200; catalog #PA5-81297, Thermo Fisher Scientific), rabbit anti-Doublecortin (1:500; catalog #4604S, Cell Signalling Technology), mouse-anti-PSD95 (1:100; catalog #MAB1596, Millipore), rabbit anti-Synaptophysin (1:200; catalog #AB_443419, Abcam), mouse anti-Aβ (6E10; 1:500; catalog #803001, BioLegend), and mouse anti-Phospho-Tau (Ser202, Thr205; AT8; 1:200; catalog #MN1020, Thermo Fisher Scientific). Donkey-derived secondary antibodies conjugated with Alexa Fluor 488 (1:500; catalog #A-11034, Thermo Fisher Scientific) or Alexa Fluor 647 (1:500; catalog #A-31571, Thermo Fisher Scientific) were used for fluorescence, and DAPI (1 μg/ml, catalog #D9542, Sigma-Aldrich) was used to counterstain nuclei. Images were captured using a Leica SP8 or Zeiss LSM880 confocal microscope and subjected to quantification with ImageJ software (National Institutes of Health, https://imagej.nih.gov/ij/).

Phospho-Tau examination

The levels of Phospho-Tau (T181) were determined by the single-molecule immune detection method (AstroBio).

Behavioral Tests

Morris Water Maze. Morris Water Maze (MWM) tests were performed in a 1.2-m-diameter circular tank filled with opaque water at 22°C, using a modified protocol (Du et al., 2018). The walls surrounding the tank were marked with bright contrasting shapes that serve as spatial reference cues. A fixed platform (10 cm diameter) was placed in a selected target quadrant. During training, the platform was submerged, and the mice were placed into the maze at one of four points randomly facing the wall of the tank. Mice were allowed to search for a platform for 1 min; if the mice were unable to find the platform, they were gently guided to the platform for 10 s. Two trials a day were conducted with a minimum of a 1 h intertrial interval. On day 6, the hidden platform was removed, and a probe test was performed. Escape latency to find the platform during training and time spent in the target quadrant during the probe test were recorded and analyzed by CleverSys TopScanLite software.

Novel object recognition. Novel object recognition (NOR) consists of the following phases: habituation, training, and test (Zhao et al., 2019). On day 1, mice were habituated to an open field box (40 cm × 40 cm × 40 cm) for 5 min. On day 2, two same objects were placed in two diagonal corners of the box, and mice were put into the box and allowed to explore for 8 min. Twenty-four hours later (day 3), one of the objects was replaced with a novel object, and then mice were put back to the box and allowed to explore for 8 min. Cumulative time each mouse spent on exploring each object was recorded by TopScanLite (Clever Sys). The discrimination index was calculated as follows: discrimination index = novel object exploration time/(novel object exploration time + familiar object exploration time).

Contextual fear conditioning test. Contextual fear condition (CFC) tests were performed based on a modified protocol (Shoji et al., 2014).

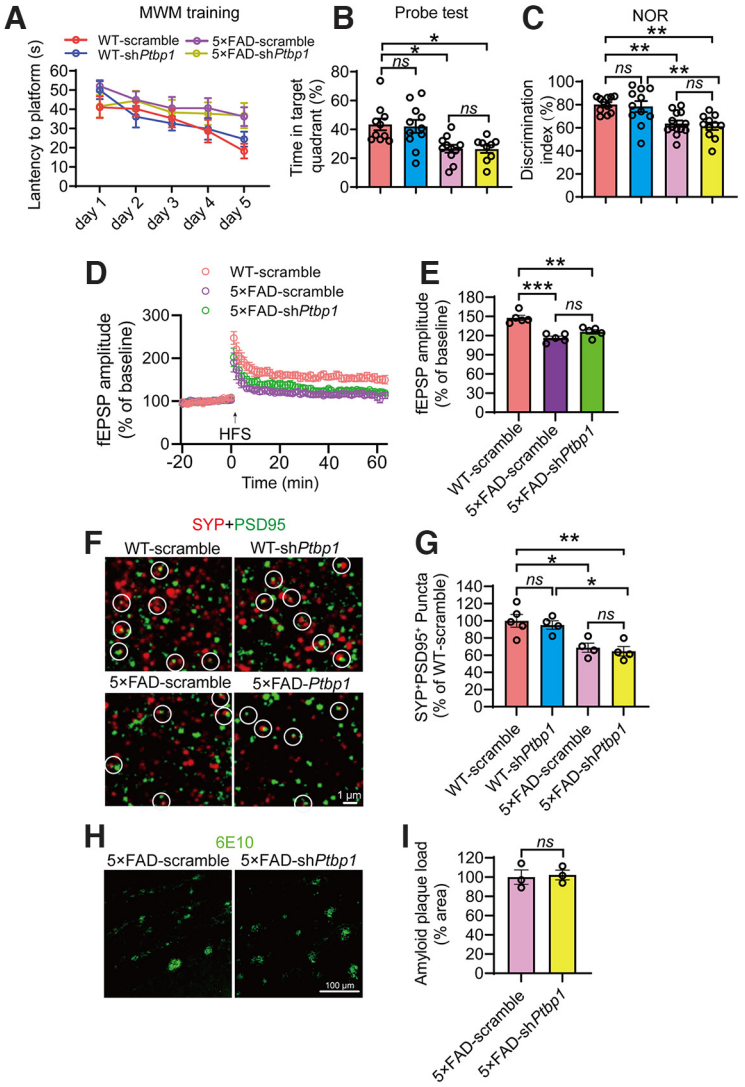

Figure 3. Downregulation of PTBP1 in the hippocampus fails to attenuate cognitive and synaptic deficits as well as Aβ deposition in 5×FAD mice. ***A***, ***B***, MWM analysis of 5×FAD and WT control mice 2.5 months after sh*Ptbp1* or the scramble control AAV transduction. The latency to find the hidden platform during the training phase (***A***), time spent in the target quadrant in the probe test (***B***); $n = 9$–11 animals, one-way ANOVA with Tukey's multiple comparisons. ***C***, Quantification of discrimination indexes in the NOR test of the experimental mouse; $n = 11$–13 animals, one-way ANOVA with Tukey's multiple comparisons. ***D***, ***E***, Electrophysiological analysis of LTP. Recordings of hippocampal LTP induced by high-frequency stimulation (HFS, ***D***), quantification of the field excitatory postsynaptic potentials (fEPSPs) during the last 10 min of LTP recording (***E***); $n = 5$ brain slices from 4 animals per group, one-way ANOVA with Tukey's multiple comparisons. ***F***, ***G***, Confocal analysis of $SYP^{+}PSD95^{+}$ synaptic puncta. Representative images (***F***), quantification (***G***); $n = 4$–5 animals, one-way ANOVA with Tukey's multiple comparisons. ***H***, ***I***, Confocal analysis of 6E10 (Aβ antibody) stained amyloid deposits. Representative images (***H***), quantification (***I***); $n = 3$ animals per group, unpaired *t* test. All quantified data are represented as mean ± SEM; $^{*}p < 0.05$, $^{**}p < 0.01$, $^{***}p < 0.001$. *ns*, Not significant.

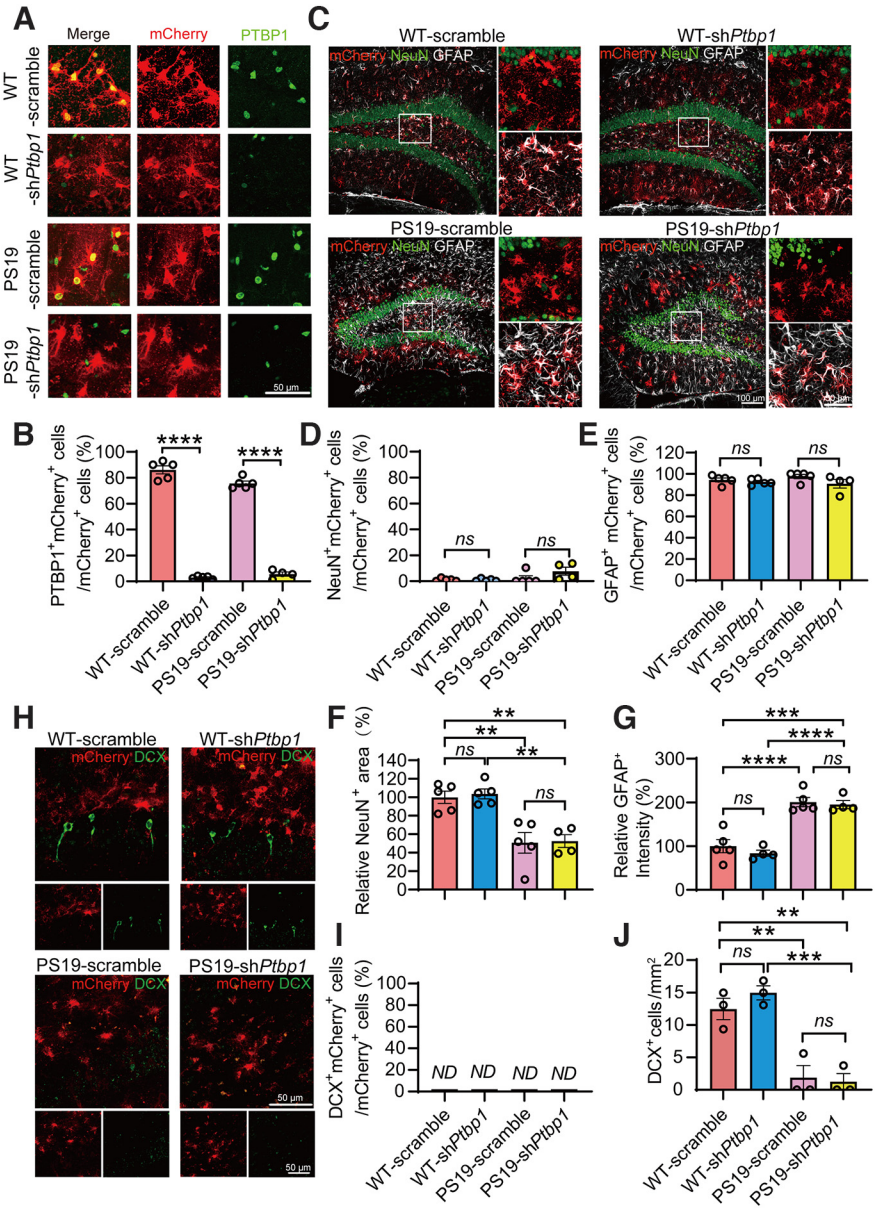

Figure 4. Knockdown of PTBP1 cannot convert astrocytes into neurons in the hippocampus of PS19 mice. ***A***, ***B***, Confocal analysis of PTBP1 expression in mCherry$^+$ cells in the hippocampus of PS19 and WT control mice 3 months after sh*Ptbp1* or the scramble control AAV transduction. Representative images (***A***), quantification (***B***); $n = 4$–5 animals, unpaired t test. ***C***–***G***, Confocal analysis of fluorescent cells. Representative images (***C***), quantification (***D***–***G***); $n = 4$–5 animals, one-way ANOVA with Tukey's multiple comparisons. ***H***–***J***, Confocal analysis of mCherry$^+$ cells and DCX$^+$ cells. Representative images (***H***), quantification (***I***, ***J***); $n = 3$ animals per group, one-way ANOVA with Tukey's multiple comparisons. All quantified data are represented as mean ± SEM; $^{**}p < 0.01$, $^{***}p < 0.001$, $^{****}p < 0.0001$. *ns*, Not significant; *ND*, not detectable.

On day 1, mice were placed into a conditioning box with a metal plate and allowed to explore the box freely for 2 min for habituation. Thereafter, mice received a 2 s electric foot shock (0.5 mA) three times, with a 1 min interval between each shock. Mice were left in the box for an additional min after the final electric shock. For the contextual test, mice were re-exposed to the same conditioning box for 5 min, 14 d after training. Time of freezing behavior for each mouse was analyzed by CleverSys FreezeScan. The freezing percentage was calculated as follows: freezing % = (freezing time/total time) during the test – (freezing time/total time) during habitation.

Electrophysiology

For analysis of long-term potentiation (LTP), *ex vivo* hippocampal slices were prepared from 10-month-old wild-type (WT) and 5×FAD mice at 3 months post-transduction of AAV-sh*Ptbp1* or AAV-scramble. All the subsequent procedures are the same as described previously (Zheng et al., 2021).

Statistical analysis

Quantification results are displayed as mean ± SEM. Sample sizes are comparable to those described previously in similar studies (Qian et al., 2020; Wang et al., 2021), although statistical methods were not used to predetermine sample sizes in this study. Details for sample sizes and statistical tests can be found in the figure legends. Statistical analyses were performed with GraphPad Prism software (version 9.0, https://www.graphpad.com/). Differences were assessed by unpaired t tests or one-way ANOVA where appropriate, and p values < 0.05 were considered statistically significant.

Results

Knockdown of PTBP1 by an astrocyte-restrictive AAV shRNA fails to convert hippocampal astrocytes into neurons *in vivo*

AAV driven by specific promoters has been widely used to efficiently deliver genes or DNA fragments including shRNAs into particular types of CNS cells. We constructed an *hGFAP* promoter-driven AAV vector, which comprises a mCherry reporter and a *Ptbp1*-targeting shRNA in an miR30 cassette (Fig. 1*A*). A modified longer form of *hGFAP* promoter was used to ensure the specificity of astrocytic expression, as many serotypes of the AAV driven by the short form *hGFAP* promoter have been reported to have leaky expression in nonastrocytic cells (Wang et al., 2021). The knockdown efficiency of three AAV shRNA viruses was compared with the control AAV scramble virus in primary astrocytic cultures. Because of the highest knockdown efficiency of AAV-GFAP-sh*Ptbp1*-1 ($F_{(3,8)} = 64.04$, $p < 0.0001$, one-way ANOVA; Fig. 1*B*, *C*; nucleotide sequence of the shRNA is identical to that used in Qian et al., 2020), it was chosen and designated as AAV-sh*Ptbp1* or sh*Ptbp1* for all subsequent experiments.

We next transduced AAV-sh*Ptbp1* unilaterally into the right hippocampal dentate gyrus, and AAV-scramble control in the left dentate gyrus of adult WT mice (Fig. 1*D*). Two weeks after the transduction, both sides showed restricted mCherry expression in GFAP$^+$ astrocytes in the dentate gyrus and the nearby areas ($t_{(6)} = 0.4552$, $p = 0.665$, unpaired t test; Fig. 1*E*–*G*). IF staining for PTBP1 showed that AAV-sh*Ptbp1* achieved nearly complete depletion of PTBP1 in mCherry$^+$ cells and, consequently, a dramatic reduction in the number of PTBP1$^+$mCherry$^+$ cells when

compared with the control side ($t_{(6)}$ = 36.16, $p < 0.0001$, unpaired t test; Fig. 1*H*,*I*). These results demonstrate that AAV-sh*Ptbp1* can rapidly, efficiently, and specifically knock down PTBP1 in the hippocampal astrocytes *in vivo*. Nevertheless, AAV-sh*Ptbp1* yielded only a handful and negligible numbers of NeuN$^+$mCherry$^+$ cells, which are similar to AAV-scramble control ($t_{(6)}$ = 0, $p > 0.9999$, unpaired t test; Fig. 1*J*,*K*). DCX$^+$mCherry$^+$ cells were undetectable, whereas the numbers of DCX$^+$ cells were comparable in the knockdown and control groups ($t_{(6)}$ = 0.2094, p = 0.8411, unpaired t test; Fig. 1*J*,*L*,*M*). Our data clearly show that suppression of PTBP1 expression cannot convert astrocytes into either immature or mature neurons.

Sustained downregulation of PTBP1 fails to convert hippocampal astrocytes into neurons in an amyloid AD mouse model

Next, we investigated whether a long-term and continuous PTBP1 downregulation can enhance neuronal generation in 5×FAD mice, a widely used AD mouse model with progressive amyloid-β (Aβ) pathology and synaptic and cognitive impairments (Guo et al., 2020). The long-term knockdown of PTBP1 strategy was based on the fact that the astrocyte-to-neuron conversion as well as the pathogenesis of most neurodegenerative diseases such as AD and PD are progressive and chronic. We injected AAV-sh*Ptbp1* or AAV-scramble bilaterally into the hippocampus of 5×FAD and WT control mice at ~5.5 months of age and performed IF analyses at 1 and up to 3 months after the transduction. AAV-sh*Ptbp1* markedly reduced the expression of PTBP1 in mCherry$^+$ cells when compared with the AAV-scramble group (1 M, $F_{(3,8)}$ = 1017, $p < 0.0001$, one-way ANOVA; 3 M, $F_{(3,14)}$ = 361.4, $p < 0.0001$, one-way ANOVA; Fig. 2*A*,*B*). However, only a neglectable fraction of NeuN$^+$mCherry$^+$ cells were observed, whereas the vast majority of mCherry$^+$ cells are GFAP$^+$ astrocytes (NeuN$^+$mCherry$^+$/mCherry$^+$, 1 M, $F_{(3,8)}$ = 0.6319, p = 0.6148, one-way ANOVA; 3 M, $F_{(3,13)}$ = 0.6705, p = 0.5852, one-way ANOVA; GFAP$^+$mCherry$^+$/mCherry$^+$, 1 M, $F_{(3,8)}$ = 0.04,989, p = 0.9842, one-way ANOVA; 3 M, $F_{(3,13)}$ = 1.207, p = 0.3462, one-way ANOVA; Fig. 2*C*–*E*). In addition, NeuN$^+$ areas did not vary between AAV-sh*Ptbp1* and AAV-scramble groups (1 M, $F_{(3,8)}$ = 0.2185, p = 0.8809, one-way ANOVA; 3 M, $F_{(3,13)}$ = 0.5026, p = 0.6871, one-way ANOVA; Fig. 2*C*,*F*). Further, AAV-sh*Ptbp1* failed to reverse the overproliferation of GFAP$^+$ astrocytes and the reduction of DCX$^+$ cells in 5×FAD mice (GFAP$^+$ astrocytes, 1 M, $F_{(3,8)}$ = 54.02, $p < 0.0001$, one-way ANOVA; 3 M, $F_{(3,13)}$ = 9.367, p = 0.0015, one-way ANOVA; DCX$^+$ cells, 1 M, $F_{(3,9)}$ = 7.748, p = 0.0073, one-way ANOVA; 3 M, $F_{(3,8)}$ = 9.908, p = 0.0045, one-way ANOVA; Fig. 2*C*,*G*–*I*), two phenomena that have been reported (Demars et al., 2010; Perez-Nievas and Serrano-Pozo, 2018; Zaletel et al., 2018). DCX$^+$mCherry$^+$ cells were completely undetectable in all groups (Fig. 2*H*,*J*). Together, these results demonstrate that sustained downregulation of PTBP1 in the hippocampus also fails to convert astrocytes into neurons in 5×FAD mice.

PTBP1 downregulation cannot alleviate Aβ-associated synaptic and cognitive deficits and pathologies in AD mice

The ultimate goal for neuronal regeneration is to restore brain functions that are impaired in neurodegeneration. We performed behavioral tests to evaluate cognitive functions of the mice after AAV-mediated PTBP1 knockdown. In the Morris Water Maze test, AAV-sh*Ptbp1* failed to alleviate the deficits of spatial memory in 5×FAD mice in the training and probe test

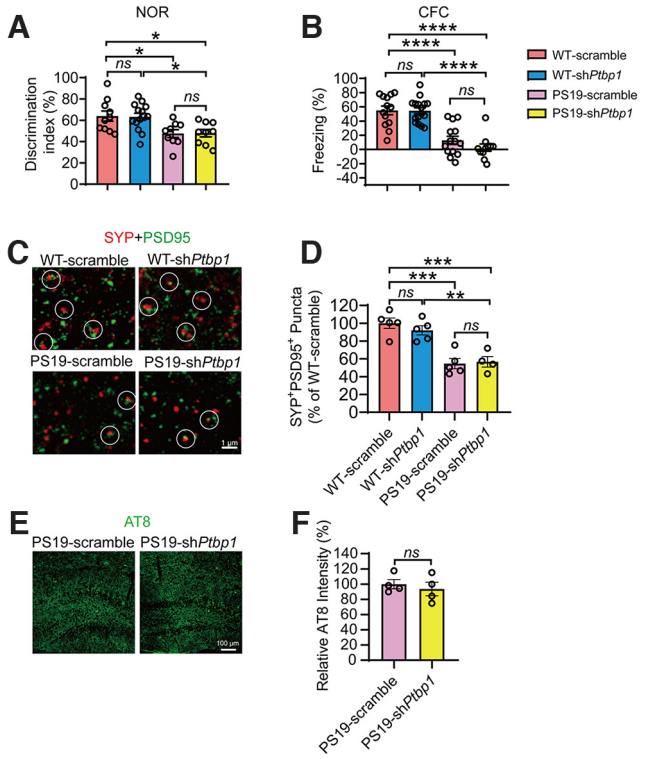

Figure 5. Downregulation of PTBP1 in the hippocampus fails to attenuate cognitive and synaptic deficits as well as tau pathology in PS19 mice. ***A***, Quantification of discrimination indexes in the NOR test of PS19 and WT control mice 2.5 months after the sh*Ptbp1* or the scramble control AAV transduction; n = 9–14 animals, one-way ANOVA with Tukey's multiple comparisons. ***B***, Analysis of the freezing behavior of the experimental mouse during the CFC test; n = 11–16 animals, one-way ANOVA with Tukey's multiple comparisons. ***C***, ***D***, Confocal analysis of SYP$^+$PSD95$^+$ synaptic puncta. Representative images (***C***), quantification (***D***); n = 4–5 animals, one-way ANOVA with Tukey's multiple comparisons. ***E***, ***F***, Confocal analysis of AT8 (phospho-tau antibody) stained tau pathology. Representative images (***E***), quantification (***F***); n = 4 animals per group, unpaired t test. All quantified data are represented as mean ± SEM; *$p < 0.05$, **$p < 0.01$, ***$p < 0.001$, ****$p < 0.0001$. *ns*, Not significant.

phases ($F_{(3,37)}$ = 6.631, p = 0.0011, one-way ANOVA; Fig. 3*A*,*B*). Similarly, the NOR test showed that compared to the WT control mice, 5×FAD mice spent less time on the novel object, and AAV-sh*Ptbp1* was unable to reverse this deficit ($F_{(3,42)}$ = 8.906, p = 0.0001, one-way ANOVA; Fig. 3*C*). As expected, AAV-sh*Ptbp1* also failed to rescue impairments in LTP and synaptophysin (SYP)/PSD95-labeled synaptic clusters in 5×FAD mice ($F_{(2,12)}$ = 21.11, p = 0.0001, one-way ANOVA; $F_{(3,13)}$ = 8.715, p = 0.0020, one-way ANOVA; Fig. 3*D*–*G*). Additionally, amyloid deposition in the hippocampus of 5×FAD mice was not altered after PTBP1 downregulation ($t_{(4)}$ = 0.2397, p = 0.8223, unpaired t test; Fig. 3*H*,*I*). Together, PTBP1 downregulation can neither restore synaptic and cognitive function nor reduce amyloid pathology in 5×FAD mice.

Knockdown of PTBP1 fails to induce the hippocampal astrocyte-to-neuron conversion and improve cognitive function in tau transgenic mice

Tau pathology has been linked to the degree of dementia and is considered to play a causal role in neuronal loss in tauopathies including AD (Fu et al., 2017; Guo et al., 2020). We therefore assessed the PTBP1 knockdown strategy in tau transgenic PS19 mice that develop neuronal loss and brain atrophy starting at 9 months (Yoshiyama et al., 2007). AAV-sh*Ptbp1* or AAV-

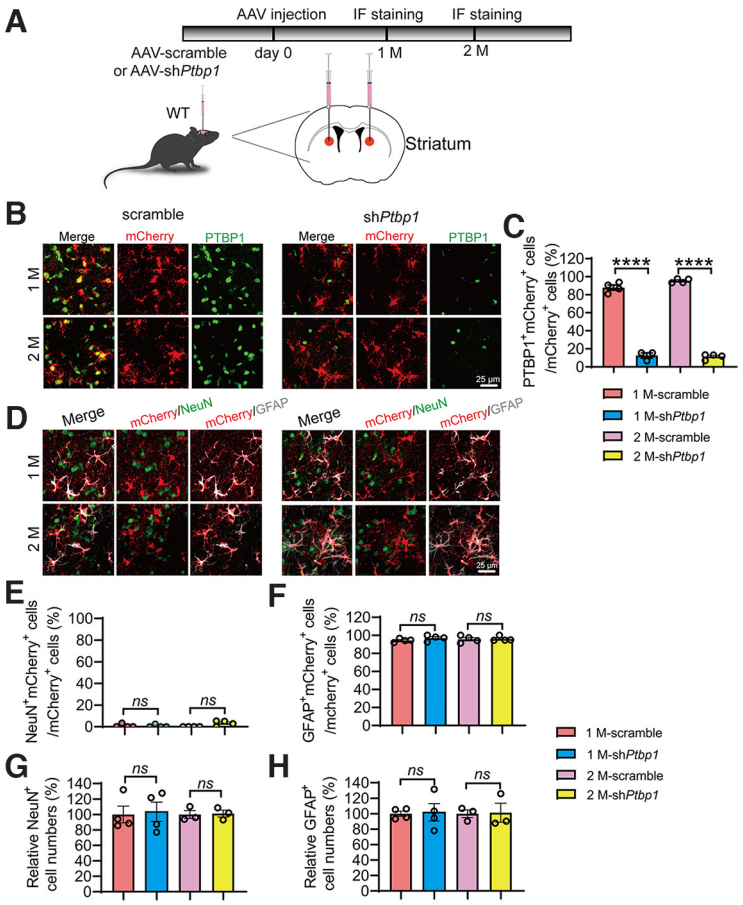

Figure 6. Knockdown of PTBP1 cannot convert astrocytes into neurons in the mouse striatum. ***A***, Schematic of study design. ***B***, ***C***, Confocal analysis of PTBP1 expression in mCherry$^+$ cells. Representative images (***B***), quantification (***C***); $n = 3$–4 animals, one-way ANOVA with Tukey's multiple comparisons. ***D***–***H***, Confocal analysis of fluorescent cells. Representative images (***D***), quantification (***E***–***H***); $n = 3$–4 animals, one-way ANOVA with Tukey's multiple comparisons. All quantified data are represented as mean ± SEM; ****$p < 0.0001$. *ns*, Not significant.

scramble viruses were injected bilaterally into the hippocampus of 8-month-old PS19 and WT mice. Similar to the 5×FAD mice tested above, the expression of PTBP1 was dramatically reduced in mCherry$^+$ cells 3 months after AAV-sh*Ptbp1* transduction ($F_{(3,15)} = 472.2$, $p < 0.0001$, one-way ANOVA; Fig. 4*A*,*B*). mCherry fluorescent signals were detected mostly in GFAP$^+$ astrocytes, sparsely in NeuN$^+$ neurons, and were undetectable in DCX$^+$ cells in both AAV-sh*Ptbp1* and AAV-scramble groups ($F_{(3,15)} = 3.171$, $p = 0.0551$, one-way ANOVA; $F_{(3,15)} = 1.501$, $p = 0.2548$, one-way ANOVA; Fig. 4*C*–*E*,*H*,*I*). Consistent with the previous reports (Yoshiyama et al., 2007), we expectedly observed the apparent loss of NeuN$^+$ mature neurons and DCX$^+$ neuronal progenitors, as well as increased GFAP$^+$ astrocytes in PS19 mice, all of which, however, remained completely unaffected following the efficient PTBP1 downregulation ($F_{(3,15)} = 13.22$, $p = 0.0002$, one-way ANOVA; $F_{(3,14)} = 28.59$, $p < 0.0001$, one-way ANOVA; $F_{(3,8)} = 22.54$, $p = 0.0003$, one-way ANOVA; Fig. 4*C*,*F*–*H*,*J*).

Cognitive function of PS19 and WT mice transduced with AAV-sh*Ptbp1* or AAV-scramble were also assessed. In the NOR test, PS19 mice spent significantly less time on the novel object when compared with the WT control groups; and downregulation of PTBP1 did not improve this performance ($F_{(3,38)} = 5.514$, $p = 0.0030$, one-way ANOVA; Fig. 5*A*). We next used the CFC test to examine memory decay and found that AAV-sh*Ptbp1* failed to rescue the deficits of PS19 mice in freezing behaviors when examined 2 weeks after the initial electric shock ($F_{(3,50)} = 25.98$, $p < 0.0001$, one-way ANOVA; Fig. 5*B*). In addition, we surveyed synapses and tau pathology in PS19 mice and found that loss of SYP$^+$PSD95$^+$ synaptic clusters and the presence of AT8$^+$ phosphor-tau deposition remained and were not alleviated by PTBP1 knockdown ($F_{(3,15)} = 17.26$, $p < 0.0001$, one-way ANOVA; $t_{(6)} = 0.5935$, $p = 0.5745$, unpaired *t* test; Fig. 5*C*–*F*. The levels of tau phosphorylated at T181 site were also not altered (data not shown).

Together, our results clearly show that downregulation of PTBP1 in hippocampal astrocytes fails to convert astrocytes into neurons and consequently are unable to improve cognitive function in mice under either physiological or pathologic conditions associated with AD.

Downregulation of PTBP1 fails to convert astrocytes into neurons in either striatum or substantia nigra of mice

To investigate whether brain-region specificity exists for the presumed astroglia-to-neuron conversion induced by PTBP1 downregulation, we injected AAV-sh*Ptbp1* or AAV-scramble viruses into the striatum or substantia nigra of the adult mice, the two brain regions in which a successful astrocyte-to-neuron conversion by downregulating PTBP1 has been claimed (Qian et al., 2020; Zhou et al., 2020). In our study, similar to the hippocampus, astrocytic PTBP1 expression was nearly completely downregulated by AAV-sh*Ptbp1* in the striatum 1 or 2 months after the viral injection ($F_{(3,11)} = 467.2$, $p < 0.0001$, one-way ANOVA; Fig. 6*A*–*C*). However, we found that only a neglectable portion of mCherry$^+$ cells were NeuN$^+$, whereas most of mCherry$^+$ cells were GFAP$^+$ ($F_{(3,12)} = 3.182$, $p = 0.0631$, one-way ANOVA; $F_{(3,12)} = 0.5198$, $p = 0.6766$, one-way ANOVA; Fig. 6*D*–*F*), indicative of a complete failure of astrocyte-to-neuron conversion. In addition, the numbers of NeuN$^+$ or GFAP$^+$ cells near the injection site were indistinguishable between AAV-sh*Ptbp1* and the control AAV-scramble groups ($F_{(3,10)} = 0.0286$, $p = 0.9930$, one-way ANOVA; $F_{(3,10)} = 0.01{,}095$, $p = 0.9983$, one-way ANOVA; Fig. 6*G*,*H*).

Similar results were obtained in the substantia nigra region. An efficient knockdown of PTBP1 in astrocytes did not result in any significant differences in the numbers of NeuN$^+$mCherry$^+$, GFAP$^+$mCherry$^+$, NeuN$^+$, and GFAP$^+$ cells when compared with the scramble control group ($F_{(3,14)} = 882.5$, $p < 0.0001$, one-way ANOVA; $F_{(3,10)} = 1.073$, $p = 0.4039$, one-way ANOVA; $F_{(3,10)} = 0.4861$, $p = 0.6995$, one-way ANOVA; $F_{(3,8)} = 0.08{,}626$, $p = 0.9656$, one-way ANOVA; $F_{(3,10)} = 0.3536$, $p = 0.7876$, one-way ANOVA; Fig. 7*A*–*H*). Together, our data clearly demonstrate that downregulation of PTBP1 is unable to convert astrocytes into neurons in all brain regions tested including the hippocampus, the striatum, and the substantia nigra.

Discussion

Having efficiently downregulated PTBP1 in the astrocytes in combination with cell lineage analyses, we fail to observe any glia-to-neuron conversion induced by PTBP1 knockdown in multiple rodent brain regions at different ages, under either physiological or pathologic conditions associated with AD. Similar to what we have found, a recent study also failed to replicate the reported astrocyte-to-neuron conversion as a result of PTBP1 knockdown (Wang et al., 2021). In the same study, Wang et al. (2021) observed a dramatically increased number of $NeuN^+$ $mCherry^+$ cells in the mouse brain transduced with astrocyte-restrictive AAV expressing mCherry reporter and NeuroD1. They therefore used stringent lineage tracing strategies to investigate the origin of the increased $NeuN^+mCherry^+$ cells and revealed that they are in fact endogenous neurons that were experimentally labeled with mCherry because of altered cell-type specificity of the AAV virus induced by NeuroD1 overexpression. Because we found no evidence for neuronal generation induced by PTBP1 downregulation, it is therefore unnecessary to perform the lineage tracing analysis.

The discrepancies among the findings from Fu-Yang labs, our lab, and Zhang labs are not likely because of differentially viral toxicities because similar titers of AAV were used in all studies; instead, the differential leakage of astrocytic labeling systems would be more likely (Qian et al., 2020; Zhou et al., 2020; Wang et al., 2021). Our AAV driven by the long-form *hGFAP* promoter showed extremely low leaky expression in neurons. Apparent neuronal leakage of Cre expression in neuronal cells has been well documented in the *mGfap-Cre* line (Wang et al., 2021), which was used in the Qian et al. (2020) study. Specifically, a control for PTBP1 downregulation was missed in the experiments evaluating astrocyte-to-neuron conversion *in vivo* (Qian et al., 2020; Fig. 2*B–H*, Fig. 3). Although the information pertinent to the *GFAP* promoter in AAV-CasRx plasmids was completely missing in the Zhou et al. (2020) study, the information from Addgene (https://www.addgene.org/154001/ and https://www.addgene.org/154000/) shows that these plasmids make up a short-form *GFAP* promoter. Wang et al. (2021), however, was not able to downregulate PTBP1 and hence trigger glia-to-neuron conversion using the same AAV-CasRx system. In addition, we observed that PTBP1 predominantly localizes in the nucleus, a subcellular compartment for RNA-binding proteins, whereas PTBP1 was detected all over the cell without a specific subcellular localization in the Zhou et al. (2020) study.

The definitive aim of neuronal regeneration is to improve, if not completely restore, brain functions deteriorated in neurodegeneration. Synaptic failure, a primary cause for cognitive impairment in AD, ought to be rescued if nascent neurons would be replenished from the resident glia cells. Our results demonstrate that PTBP1 downregulation in astrocytes cannot improve cognitive and synaptic function through any mechanisms including the neuronal regeneration. However, we do not exclude the possibility that PTBP1 in other types of cells can regulate cognitive function. A recent study reported that injection of ASO targeting *Ptbp1* into CSF in 1.5-year-old mice could improve their cognitive function (Maimon et al., 2021). Because of small sample sizes (n = 3–5 mice per group) of behavioral assays in this study, the beneficial effect of PTBP1 downregulation on cognitive function needs to be validated in future studies. In addition, because the ASO system lacks cellular specificity, it is possible that PTBP1 was downregulated in multiple cell types within the CNS. Further investigations are required to elucidate cellular distribution of ASOs from CSF injection and PTBP1 in which cell types may modulate cognitive function.

However, we do not exclude the possibility that PTBP1 downregulation could improve other brain functions such as motor

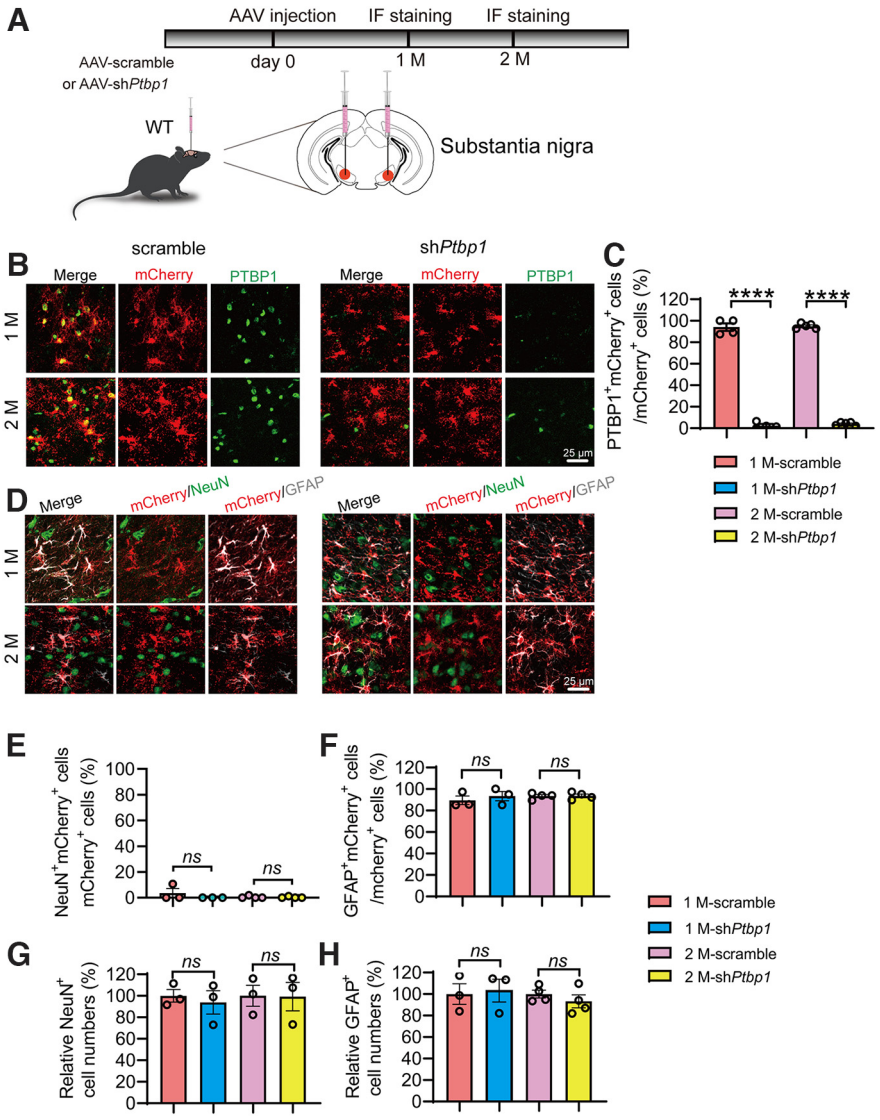

Figure 7. Downregulation of PTBP1 cannot convert astrocytes into neurons in the mouse substantia nigra. ***A***, Schematic of study design. ***B***, ***C***, Confocal analysis of PTBP1 expression in $mCherry^+$ cells. Representative images (***B***), quantification (***C***); n = 4–5 animals, one-way ANOVA with Tukey's multiple comparisons. ***D–H***, Confocal analysis of fluorescent cells. Representative images (***D***), quantification (***E–H***); n = 3–4 animals, one-way ANOVA with Tukey's multiple comparisons. All quantified data are represented as mean ± SEM; ****$p < 0.0001$. *ns*, Not significant.

function, which has been shown previously (Qian et al., 2020; Zhou et al., 2020). Future experiments are required to more carefully and in greater detail test the strategy targeting PTBP1 in treating neurodegenerative diseases not only in rodents but also primates.

References

Challis RC, Ravindra Kumar S, Chan KY, Challis C, Beadle K, Jang MJ, Kim HM, Rajendran PS, Tompkins JD, Shivkumar K, Deverman BE, Gradinaru V (2019) Systemic AAV vectors for widespread and targeted gene delivery in rodents. Nat Protoc 14:379–414.

Chen YC, Ma NX, Pei ZF, Wu Z, Do-Monte FH, Keefe S, Yellin E, Chen MS, Yin JC, Lee G, Minier-Toribio A, Hu Y, Bai YT, Lee K, Quirk GJ, Chen G (2020) A NeuroD1 AAV-based gene therapy for functional brain repair after ischemic injury through *in vivo* astrocyte-to-neuron conversion. Mol Ther 28:217–234.

Demars M, Hu YS, Gadadhar A, Lazarov O (2010) Impaired neurogenesis is an early event in the etiology of familial Alzheimer's disease in transgenic mice. J Neurosci Res 88:2103–2117.

Du Y, Zhao Y, Li C, Zheng Q, Tian J, Li Z, Huang TY, Zhang W, Xu H (2018) Inhibition of PKCδ reduces amyloid-β levels and reverses Alzheimer disease phenotypes. J Exp Med 215:1665–1677.

Fu H, Rodriguez GA, Herman M, Emrani S, Nahmani E, Barrett G, Figueroa HY, Goldberg E, Hussaini SA, Duff KE (2017) Tau pathology induces excitatory neuron loss, grid cell dysfunction, and spatial memory deficits reminiscent of early Alzheimer's disease. Neuron 93:533–541.e5.

Gage FH (2019) Adult neurogenesis in mammals. Science 364:827–828.

Grande A, Sumiyoshi K, López-Juárez A, Howard J, Sakthivel B, Aronow B, Campbell K, Nakafuku M (2013) Environmental impact on direct neuronal reprogramming *in vivo* in the adult brain. Nat Commun 4:2373.

Guo T, Zhang D, Zeng Y, Huang TY, Xu H, Zhao Y (2020) Molecular and cellular mechanisms underlying the pathogenesis of Alzheimer's disease. Mol Neurodegener 15:40.

Guo Z, Zhang L, Wu Z, Chen Y, Wang F, Chen G (2014) *In vivo* direct reprogramming of reactive glial cells into functional neurons after brain injury and in an Alzheimer's disease model. Cell Stem Cell 14:188–202.

Kalia LV, Lang AE (2015) Parkinson's disease. Lancet 386:896–912.

Kempermann G, Gage FH, Aigner L, Song H, Curtis MA, Thuret S, Kuhn HG, Jessberger S, Frankland PW, Cameron HA, Gould E, Hen R, Abrous DN, Toni N, Schinder AF, Zhao X, Lucassen PJ, Frisén J (2018) Human adult neurogenesis: evidence and remaining questions. Cell Stem Cell 23:25–30.

Lentini C, d'Orange M, Marichal N, Trottmann MM, Vignoles R, Foucault L, Verrier C, Massera C, Raineteau O, Conzelmann KK, Rival-Gervier S, Depaulis A, Berninger B, Heinrich C (2021) Reprogramming reactive glia into interneurons reduces chronic seizure activity in a mouse model of mesial temporal lobe epilepsy. Cell Stem Cell 28:2104–2121.e10.

Liu Y, Miao Q, Yuan J, Han S, Zhang P, Li S, Rao Z, Zhao W, Ye Q, Geng J, Zhang X, Cheng L (2015) Ascl1 converts dorsal midbrain astrocytes into functional neurons *in vivo*. J Neurosci 35:9336–9355.

Maimon R, Chillon-Marinas C, Snethlage CE, Singhal SM, McAlonis-Downes M, Ling K, Rigo F, Bennett CF, Da Cruz S, Hnasko TS, Muotri AR, Cleveland DW (2021) Therapeutically viable generation of neurons with antisense oligonucleotide suppression of PTB. Nat Neurosci 24:1089–1099.

Matsuda T, Irie T, Katsurabayashi S, Hayashi Y, Nagai T, Hamazaki N, Adefuin AMD, Miura F, Ito T, Kimura H, Shirahige K, Takeda T, Iwasaki K, Imamura T, Nakashima K (2019) Pioneer factor NeuroD1 rearranges transcriptional and epigenetic profiles to execute microglia-neuron conversion. Neuron 101:472–485.e7.

Mattugini N, Bocchi R, Scheuss V, Russo GL, Torper O, Lao CL, Götz M (2019) Inducing different neuronal subtypes from astrocytes in the injured mouse cerebral cortex. Neuron 103:1086–1095.e5.

Mesulam MM (1999) Neuroplasticity failure in Alzheimer's disease: bridging the gap between plaques and tangles. Neuron 24:521–529.

Mu Y, Gage FH (2011) Adult hippocampal neurogenesis and its role in Alzheimer's disease. Mol Neurodegener 6:85.

Niu W, Zang T, Smith DK, Vue TY, Zou Y, Bachoo R, Johnson JE, Zhang CL (2015) SOX2 reprograms resident astrocytes into neural progenitors in the adult brain. Stem Cell Reports 4:780–794.

Olanow CW, Goetz CG, Kordower JH, Stoessl AJ, Sossi V, Brin MF, Shannon KM, Nauert GM, Perl DP, Godbold J, Freeman TB (2003) A double-blind controlled trial of bilateral fetal nigral transplantation in Parkinson's disease. Ann Neurol 54:403–414.

Perez-Nievas BG, Serrano-Pozo A (2018) Deciphering the astrocyte reaction in Alzheimer's disease. Front Aging Neurosci 10:114.

Qian H, Kang X, Hu J, Zhang D, Liang Z, Meng F, Zhang X, Xue Y, Maimon R, Dowdy SF, Devaraj NK, Zhou Z, Mobley WC, Cleveland DW, Fu XD (2020) Reversing a model of Parkinson's disease with *in situ* converted nigral neurons. Nature 582:550–556.

Schildge S, Bohrer C, Beck K, Schachtrup C (2013) Isolation and culture of mouse cortical astrocytes. J Vis Exp 2013:50079.

Shoji H, Takao K, Hattori S, Miyakawa T (2014) Contextual and cued fear conditioning test using a video analyzing system in mice. J Vis Exp 2014:50871.

Tai W, Wu W, Wang LL, Ni H, Chen C, Yang J, Zang T, Zou Y, Xu XM, Zhang CL (2021) *In vivo* reprogramming of NG2 glia enables adult neurogenesis and functional recovery following spinal cord injury. Cell Stem Cell 28:923–937.e4.

Torper O, Ottosson DR, Pereira M, Lau S, Cardoso T, Grealish S, Parmar M (2015) *In vivo* reprogramming of striatal NG2 glia into functional neurons that integrate into local host circuitry. Cell Rep 12:474–481.

Trounson A, McDonald C (2015) Stem cell therapies in clinical trials: progress and challenges. Cell Stem Cell 17:11–22.

Wang LL, Serrano C, Zhong X, Ma S, Zou Y, Zhang CL (2021) Revisiting astrocyte to neuron conversion with lineage tracing *in vivo*. Cell 184:5465–5481.e16.

Wang X, et al. (2013) Loss of sorting nexin 27 contributes to excitatory synaptic dysfunction by modulating glutamate receptor recycling in Down's syndrome. Nat Med 19:473–480.

Wang ZF, Li HL, Li XC, Zhang Q, Tian Q, Wang Q, Xu H, Wang JZ (2006) Effects of endogenous beta-amyloid overproduction on tau phosphorylation in cell culture. J Neurochem 98:1167–1175.

Yoshiyama Y, Higuchi M, Zhang B, Huang SM, Iwata N, Saido TC, Maeda J, Suhara T, Trojanowski JQ, Lee VM (2007) Synapse loss and microglial activation precede tangles in a P301S tauopathy mouse model. Neuron 53:337–351.

Zaletel I, Schwirtlich M, Perović M, Jovanović M, Stevanović M, Kanazir S, Puškaš N (2018) Early impairments of hippocampal neurogenesis in 5xFAD mouse model of Alzheimer's disease are associated with altered expression of SOXB transcription factors. J Alzheimers Dis 65:963–976.

Zeng F, et al. (2019) The deubiquitinase USP6 affects memory and synaptic plasticity through modulating NMDA receptor stability. PLoS Biol 17: e3000525.

Zhao D, et al. (2019) RPS23RG1 is required for synaptic integrity and rescues Alzheimer's disease-associated cognitive deficits. Biol Psychiatry 86:171–184.

Zhao Y, Tseng IC, Heyser CJ, Rockenstein E, Mante M, Adame A, Zheng Q, Huang T, Wang X, Arslan PE, Chakrabarty P, Wu C, Bu G, Mobley WC, Zhang YW, St George-Hyslop P, Masliah E, Fraser P, Xu H (2015) Appoptosin-mediated caspase cleavage of tau contributes to progressive supranuclear palsy pathogenesis. Neuron 87:963–975.

Zheng Q, Li G, Wang S, Zhou Y, Liu K, Gao Y, Zhou Y, Zheng L, Zhu L, Deng Q, Wu M, Di A, Zhang L, Zhao Y, Zhang H, Sun H, Dong C, Xu H, Wang X (2021) Trisomy 21-induced dysregulation of microglial homeostasis in Alzheimer's brains is mediated by USP25. Sci Adv 7: eabe1340.

Zhou H, et al. (2020) Glia-to-neuron conversion by CRISPR-CasRx alleviates symptoms of neurological disease in mice. Cell 181:590–603.e16.